Quantifying drug-target engagement in live cells using sulfonyl fluoride chemical probes

Lyn H. Jones[a,*], Hua Xu[b], Olugbeminiyi O. Fadeyi[c]
[a]Jnana Therapeutics, Boston, MA, United States
[b]Pfizer Inc, Medicine Design, Cambridge, MA, United States
[c]Exploratory Science Center, Merck & Co, Cambridge, MA, United States
*Corresponding author: e-mail address: ljones@jnanatx.com

Contents

Abstract

Phenotypic screening in disease-relevant models identifies small molecule hits with desirable efficacy but often with unknown modes of action. Target identification and validation are integral to successful biomedical research. Technologies are required to validate the biological target (or targets) through which a pharmacological agent is proposed to exert its effects. This work details the rational structure-based design, synthetic preparation and cell-based application of a clickable sulfonyl fluoride chemical probe to directly report on the mechanism of a series of compounds previously discovered in a reporter gene assay. Quantification of drug-target occupancy in living human

Methods in Enzymology
ISSN 0076-6879
https://doi.org/10.1016/bs.mie.2019.02.010

primary cells enabled a deeper understanding of the molecular pharmacology of the chemotype. The technology described herein should be of broad interest to those involved in chemical biology research and the drug discovery endeavor.

1. Introduction

Successful drug discovery relies heavily on rigorous, and unbiased, therapeutic target validation (Jones, 2016). Productivity in the pharmaceutical industry is plagued by attrition in Phase II where the efficacy of the candidate drug is usually tested in patients for the first time. A key reason for this derives from an incomplete picture of the pharmacokinetic-pharmacodynamic (PK-PD) relationships of the drug candidate and its target under investigation. To build confidence in translational pharmacology we have previously defined a framework that attempts to establish confidence in target validation using chemical probes, such that high quality pharmacological modulators of pathophysiologically-relevant targets are progressed through preclinical and clinical R&D (Bunnage, Chekler, & Jones, 2013). The four pillars of target validation can be framed as questions: (1) Does the compound achieve the desired concentration at the site of action? (2) Does the compound engage the therapeutic target? (3) Does engagement of the target result in the desired functional effects? (4) Does this functional pharmacology have the desired phenotypic consequences in a disease-relevant context? It is important not only to confirm that the drug under investigation engages the nominated target in the relevant location/compartment but also to quantify the relationship between drug-target occupancy and its functional consequences (i.e., between pillar 2 and 3) as this builds translational PK-PD understanding (Morgan et al., 2012).

Functional chemical probes have found a myriad of uses in chemical biology and medicinal chemistry. For example, reactivity- and activity-based probes are small molecules that possess electrophilic motifs that are designed to engage their target proteins resulting in the formation of a covalent bond (Cravatt, Wright, & Kozarich, 2008; Sanman & Bogyo, 2014). The probes also incorporate a reporter group such as a fluorescent dye that enables visualization of the protein using Western blot or imaging analysis (Fig. 1). Alternatively, an appended biotin group provides an opportunity to streptavidin-enrich low expressing adducted proteins from complex proteomes. Analytical techniques employing quantitative mass spectrometry

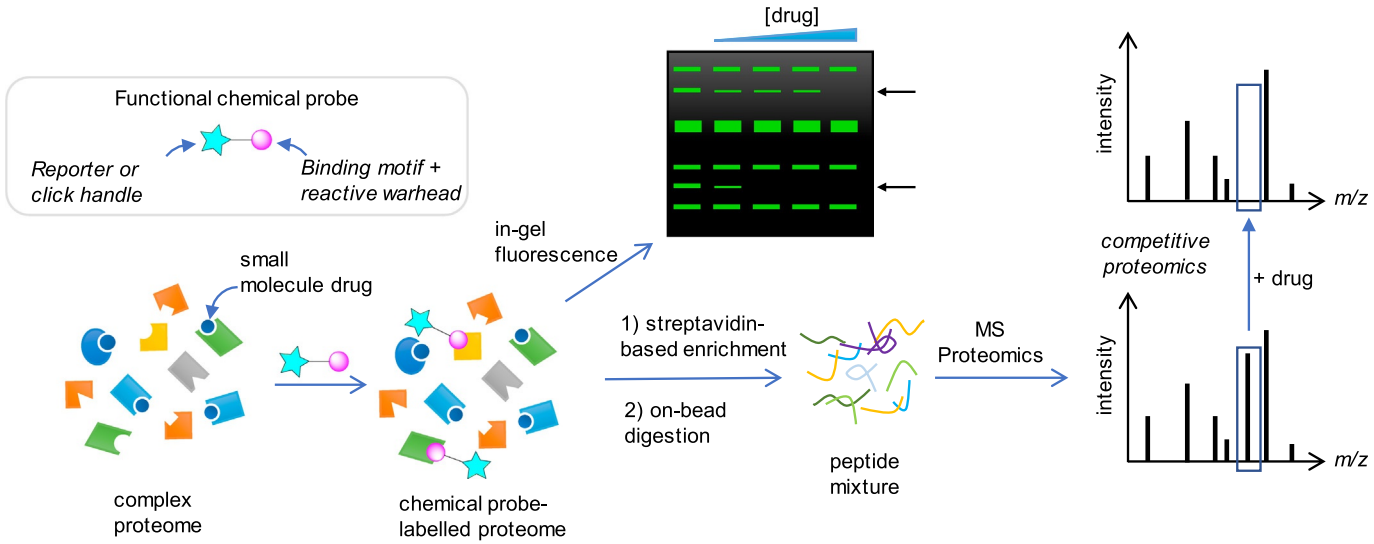

Fig. 1 General chemical probe-based labeling strategy to validate target engagement in complex proteomes.

(MS) proteomics have considerably advanced the area as they provide a simultaneous readout of multiple proteins, enabling assessments of drug selectivity in complex proteomes (Drewes & Knapp, 2018). Importantly, labeling and subsequent enrichment of the isolated protein (or proteins) can be competed by pre-incubation of the proteome with the parent drug or compound under investigation. By performing these experiments with different doses of the drug, a quantitative assessment of target occupancy is achieved (Fig. 1).

Unfortunately, the conjugation of a dye or biotin functionality to the probe perturbs its physicochemical properties that often hinders cellular permeation (significantly increasing molecular weight, hydrogen bonding capacity and electric charge) and as a result, these probes are only suitable for use in cell lysate. A more physiologically-relevant assessment of drug-target engagement is essential to understand the "true" nature of on-target occupancy and off-target selectivity. It is not unusual to observe differences in target engagement between cell lysate and intact cells and tissues. Reasons for variations in binding site occupancy include context-dependent protein-protein interactions, post-translational modifications, substrate competition and subcellular compartmentalization of the target protein, or the chemical probe itself. Technologies that assess drug-target engagement in live cells are therefore of considerable interest and are an active area of drug discovery research (Jones, 2015).

The advent of "click chemistry" has considerably advanced the area of functional chemical probe development. The concept of click chemistry was developed by Sharpless and coworkers in 2001 that refers to highly efficient, modular and often biocompatible reactions (Kolb, Finn, & Sharpless, 2001). A commonly used click reaction is the copper(I)-catalyzed azide-alkyne cycloaddition (CuAAC) that is orthogonal to other reactive biomolecular functionalities (Rostovtsev, Green, Fokin, & Sharpless, 2002; Tornøe, Christensen, & Meldal, 2002). Incorporation of one of the reaction partners (azide or alkyne) into a chemical probe does not significantly perturb its molecular weight or physicochemical properties. Reactivity-based probes that switch a dye or biotin for a "silent" click reporter such as a terminal alkyne are thus enabled for cellular permeation and use in live cells. In this workflow, cells are treated with the chemical probe, lysed and then the azide-tagged biotin or dye (or both if a bifunctional linker is used) is "clicked" onto the probe-protein adducts to mediate enrichment and analysis. As before, pre-incubation of the proteome with the drug being investigated at different concentrations and competition labeling allows target occupancy to be quantified in whole cells.

Regarding selection of the electrophilic warhead, most approaches target the highly nucleophilic cysteine residue using a variety of reactive functionalities (Liu et al., 2013). However, there are issues associated with targeting cysteine—it is difficult to achieve selectivity due to its intrinsically high nucleophilicity, and the residue is under-represented in protein functional sites. Therefore, new synthetic labeling technologies are required to target residues beyond cysteine. Sulfonyl fluoride warheads have received considerable attention in the design of chemical probes due to their ability to react with a variety of nucleophilic residues beyond cysteine (tyrosine, lysine, histidine, serine and threonine) in a context-dependent manner, i.e., residue engagement is templated (Narayanan & Jones, 2015). This is due to a need to activate the fluorine leaving group through hydrogen bonding in the microenvironment of the binding site (Dong, Krasnova, Finn, & Sharpless, 2014).

2. Target validation of the decapping scavenger enzyme (DcpS)

Spinal muscular atrophy is a rare genetic neuromuscular disease that causes muscle wasting and often leads to early death. It is caused by mutations in *SMN1* that codes for survival motor neuron (SMN) protein. Another gene, *SMN2* also codes for the SMN protein and small molecules that upregulate *SMN2* expression have therefore been of interest for the treatment of SMA. Previously, cell-based screening in a reporter gene assay identified a series of diaminoquinazoline (DAQ) derivatives that potently upregulated *SMN2* (Jarecki et al., 2005; Thurmond et al., 2008). Medicinal chemistry optimization yielded a clinical candidate RG3039, yet the biological target had not been determined at that time. Protein microarrays, that utilize glutathione S-transferase (GST)-tagged and immobilized recombinant proteins, were screened using a radiolabeled DAQ derivative and binding to a single protein, the mRNA decapping scavenger enzyme (DcpS), was identified (Singh et al., 2008). A crystal structure of related DAQ derivatives provided further evidence that the putative target was the DcpS enzyme due to their location in the mRNA cap binding pocket of the enzyme (Singh et al., 2008). However, there was no direct validation of DcpS as the target of the DAQ series in the physiologically-relevant context of human live cells. Moreover, the dibasic and lipophilic nature of RG3039 translates to lysosomal accumulation (Gopalsamy et al., 2017), a feature that has been reported to be linked to perturbation of autophagy (Ashoor, Yafawi,

Jessen, & Lu, 2013), and autophagic dysregulation is a characteristic of SMA (Garcera, Bahi, Periyakaruppiah, Arumugam, & Soler, 2013). It was therefore important to validate the in vivo efficacy of RG3039 derives from a DcpS-dependent mechanism, and not from its physicochemical properties.

Here we detail the design, synthesis and application of a clickable sulfonyl fluoride chemical probe that directly reports on DAQ-DcpS engagement in primary human peripheral blood mononuclear cells (PBMCs) (Hett et al., 2015; Xu et al., 2016). This work is representative of a chemical labeling strategy to quantify drug-target occupancy in live cells that should be of broad interest to those working in chemical biology and drug discovery research. The impact these studies had on the progression of DAQ inhibitors for the treatment of SMA is also discussed.

3. Structure-based chemical probe design

As mentioned in the Introduction, most functional chemical probes target reactive cysteine thiols, but it is an amino acid that is infrequently present in protein functional sites. In the DAQ-DcpS crystal structures there are no obviously targetable cysteine residues in the binding site (Singh et al., 2008). However, there are two tyrosine residues (Tyr113 and Tyr143) clearly proximal to DAQ ligands. Specifically, a sulfonyl fluoride motif at the *para*-position of the benzene ring would be positioned perfectly to attack Tyr143 (Fig. 2). An analysis of tyrosine residues in proteins that were found previously to fortuitously engage sulfonyl fluoride electrophiles identified a preponderance of neighboring basic residues that presumably reduce the pK_a and enhance the nucleophilicity of the phenol hydroxyl group (Hett et al., 2015). It was noticeable that in the microenvironment of the DcpS cap binding site there is a proximal lysine (Lys142) that may enhance Tyr143 reactivity (Fig. 2).

An important reason for the increased use of sulfonyl fluoride probes in chemical biology research has been the recent advances in their synthetic preparation and the availability of sulfonyl fluoride-containing reagents (Dong et al., 2014; Narayanan & Jones, 2015). Benzylation of a DAQ-phenol with *para*-fluorosulfonyl benzyl bromide readily delivered the desired probe following protecting group removal. As predicted, SF-p1 was found to be a covalent DcpS inhibitor that reacted with Tyr143 (confirmed using X-ray crystallography and peptide mapping experiments). Positioning of the click handle in the DAQ template was also enabled using structure-based design, and a terminal alkyne *ortho*- to the sulfonyl fluoride

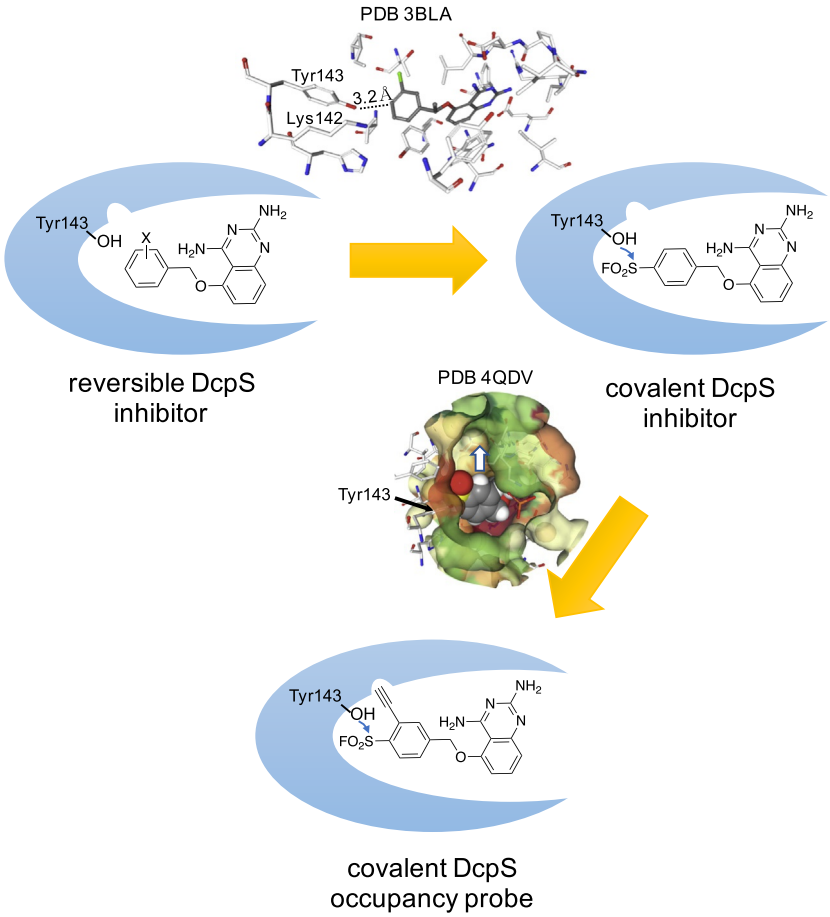

Fig. 2 Rational design of a clickable covalent chemical probe to directly measure in-cell DcpS-DAQ target engagement. The crystal structure of a reversible DAQ inhibitor with DcpS (e.g., PDB code 3BLA) shows the proximity of the *para*-position of the benzene ring to the Tyr143 hydroxy group (dotted line). The SF-p1-DcpS crystal structure (PDB code 4QDV) highlights the area of the binding pocket that can accommodate the terminal alkyne click handle (white arrow).

electrophile would appear to occupy a hydrophobic pocket in the enzyme (Fig. 2). Incorporation of the terminal alkyne relied on a palladium-mediated Stille coupling reaction with an aryl bromide derivative (performed in the presence of the sulfonyl fluoride functionality—see Section 4.4). The physicochemical properties of the resulting probe SF-p1-yne were commensurate with those of the original DAQ reversible inhibitor, thus enabling subsequent cell-based occupancy experiments.

4. Preparation of sulfonyl fluoride chemical probes

4.1 Equipment

1. Silica gel flash chromatography was performed using a medium pressure Biotage or ISCO system
2. ^{1}H, $^{13}C[^{1}H]$, and $^{19}F[^{1}H]$ NMR characterization data were collected at 300 K on a Varian 400 MHz (AS_{400}) spectrometer operating at 400.1, 100.5, and 376 MHz (respectively), or a Varian 500 MHz (AS_{500}) spectrometer operating at 500, 126, and 470 MHz (respectively)
3. IR spectra were recorded on a Nicolet Avatar 360 FT-IR spectrometer
4. High resolution mass spectroscopy (HRMS) was performed on an Agilent (6220) LC-MS TOF using an Xbridge C18 2.5 μm 3.0 × 5.0 mm
5. LC-MS was performed using an Agilent 1100 HPLC system connected to a Waters LCT Premier XE mass spectrometer
6. Peptide mapping was performed using an LTQ Orbitrap XL mass spectrometer

4.2 Chemicals

All chemicals were purchased from Sigma-Aldrich unless otherwise stated.

4.3 Synthesis of SF-p1

The synthesis of fluoride inhibitor SF-p1 is described in Fig. 3. Cyano-difluorobenzene **1** was subjected to a nucleophilic aromatic substitution (SNAr) reaction with benzyl alcohol to afford cyano-fluorobenzene derivative

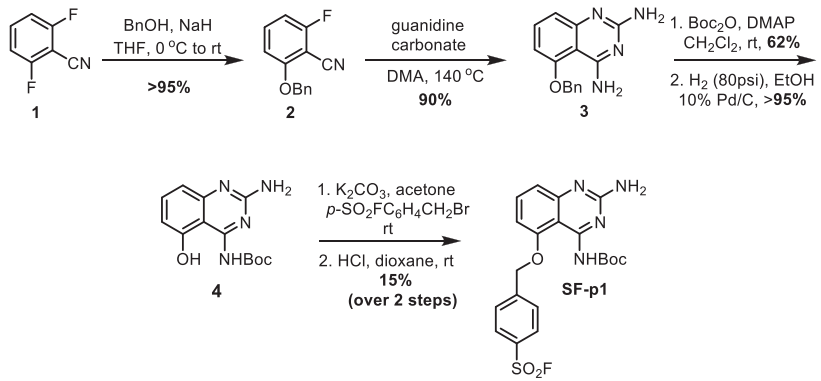

Fig. 3 Synthetic scheme for the preparation of SF-p1, a sulfonyl fluoride covalent inhibitor of DcpS

2, which was then subjected to guanidine cyclization to provide benzyl ether **3**. Boc-protection and benzyl deprotection gave the desired phenol **4**. O-alkylation with $pSO_2FC_6H_4CH_2Br$ and Boc-deprotection provided SF-p1.

1.1. Compound **4** was prepared according to the published procedure as shown in Fig. 3 (Hett et al., 2015). The key synthetic steps to provide SF-p1 are described below.

1.2. A mixture of compound **4** (80 mg, 0.288 mmol) and potassium carbonate (80 mg, 0.288 mmol) in acetone (5 mL) was allowed to stir at 50 °C for 1 h. 4-(bromomethyl)-benzenesulfonyl fluoride (188 mg, 0.6 mmol) was added to the mixture, which was then allowed to stir for 16 h at 50 °C. LC-MS showed the reaction to be complete. The mixture was filtered and purified by prep-HPLC to give *tert*-butyl 2-amino-5-(2-(fluorosulfonyl)benzyloxy)quinazolin-4-ylcarbamate as a light yellow solid (also readily purified on silica gel, 0–100% EtOAc/heptane).

1.3. This material was then dissolved in dichloromethane (5 mL) and the resulting solution was cooled to 0 °C and treated dropwise with 4 M HCl/EtOAc (0.5 mL), and allowed to stir at room temperature overnight. LC-MS showed the reaction to be complete. The mixture was concentrated and the residue was purified by prep-HPLC to give the title compound Synthesis of 2-((2,4-diaminoquinazolin-5-yloxy) methyl)benzene-5-sulfonyl fluoride (SF-p1) (15 mg, 15%) as a gray solid. ^{1}H NMR (400 MHz, CD_3OD) δ 8.12 (2H, d, $J = 8.59$ Hz), 7.85 (2H, d, $J = 8.20$ Hz), 7.67 (1H, t, $J = 8.39$ Hz), 6.99 (2H, dd, $J = 8.39$, 2.54 Hz), 5.63 (2H, s) ppm. ^{19}F NMR (376 MHz, CD_3OD) δ 64.00 ppm. ^{13}C NMR (100 MHz, CD_3OD) δ 164.6, 158.1, 156.1, 145.9, 142.9, 137.6, 134.2 (1C, d, $J = 24.9$ Hz, C-SO_2-F), 130.1, 130.1, 110.6, 108.9, 101.7, 71.1 ppm. IR (neat) 3323 (w, br), 1650 (s), 1609 (s), 1404 (m), 1213 (m), 772 (w), 597 (w) cm^{-1}. HRMS (ESI+) calcd for $C_{15}H_{14}FN_4O_3S$ $[M+H]^+$: 352.0770, found: 352.0772.

4.4 Synthesis of SF-p1-yne

The synthesis of SF-p1-yne (Fig. 4) begins with the treatment of commercially available sulfonyl chloride **5** with potassium fluoride to give the desired sulfonyl fluoride. This was subjected to carboxylic acid reduction with borane to furnish benzene sulfonyl fluoride intermediate **6** in good yield. The benzyl alcohol was subsequently converted to benzyl bromide **7** and

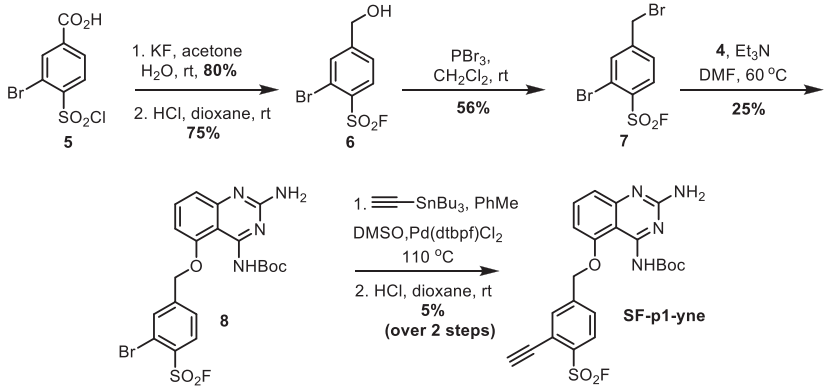

Fig. 4 Synthetic scheme for the preparation of SF-p1-yne, a clickable functional probe of DcpS occupancy.

coupled with phenol **4** to give sulfonyl fluoride intermediate **8**. The terminal alkyne was installed via Stille coupling, followed by Boc-deprotection that yielded the desired sulfonyl fluoride probe, SF-p1-yne.

2.1. To a mixture of the commercially available compound 3-bromo-4-(chlorosulfonyl)benzoic acid (**5**, 9.88 g, 33 mmol) and potassium fluoride (9.59 g, 165 mmol) was added acetone (82 mL) and water (82 mL). The reaction was stirred at room temperature overnight. The solvent was concentrated under vacuum and the residue dissolved in ethyl acetate. The organic layer was washed with brine, dried over magnesium sulfate, filtered and concentrated. The residue was purified by chromatography on silica gel eluting with a gradient of (0–50% EtOAc/heptane) to give 3-bromo-4-(fluorosulfonyl)benzoic acid (7.5 g, 80%) as a white solid. ^{1}H NMR (400 MHz, $(CD_3)_2SO$) δ 8.42 (1H, d, $J = 1.56$ Hz), 8.36 (1H, d, $J = 8.59$ Hz), 8.21 (1H, d, $J = 8.20$ Hz) ppm. ^{19}F NMR (376 MHz, $(CD_3)_2SO$) δ 58.44 (s, 1F) ppm. ^{13}C NMR (126 MHz, $(CD_3)_2SO$) δ 165.0, 139.2, 136.5, 135.9 (d, 2 JCF = 23.9 Hz), 133.3, 129.9, 120.8 ppm. IR (neat): 1702, 1510, 1417, 1305, 1281, 1214, 788, 763, 732, 618 cm^{-1}. HRMS (ESI-) m/z: calcd for $C_7H_4BrFO_4S$ $[M\text{-}H]^-$: 280.8928; found: 280.8925.

2.2. To a solution of 3-bromo-4-(fluorosulfonyl)benzoic acid (1.2 g, 4.24 mmol) in THF (17 mL) at 0 °C was added borane tetrahydrofuran complex (1.0 M in THF, 9.3 mL, 9.3 mmol) dropwise over 15 min. The reaction was gradually warmed to room temperature overnight and quenched using saturated aqueous ammonium chloride solution. The aqueous phase was extracted with EtOAc (2 × 100 mL) and the

combined organic layers were washed with brine, dried over magnesium sulfate, filtered and concentrated. The residue was purified by chromatography on silica gel (0–50% EtOAc/heptane) to give compound **6** (0.85 g, 75%) as a white solid. ^{1}H NMR (400 MHz, $(CD_3)_2SO$) δ 8.21 (1H, d, $J = 8.20$ Hz), 7.99 (1H, s), 7.69 (1H, d, $J = 8.20$ Hz), 5.66 (1H, t, $J = 5.85$ Hz), 4.66 (2H, d, $J = 5.85$ Hz) ppm. ^{19}F NMR (376 MHz, $(CD_3)_2SO$) δ 59.07 (s, 1F) ppm. ^{13}C NMR (126 MHz, $(CD_3)_2SO$) δ 154.2, 133.6, 132.8, 130.6 (d, 2 JCF = 23.94 Hz), 126.6, 120.3, 61.8 ppm. IR (neat): 3331–3247, 1591, 1413, 1350, 1211, 1049, 1029, 987, 875, 821, 773, 680, 586, 548 cm^{-1}. HRMS (ESI-) m/z: calcd for $C_7H_6BrFO_3S$ $[M\text{-}H]^-$: 266.9131; found: 266.9132.

2.3. To a solution of 2-bromo-4-(hydroxymethyl)benzenesulfonyl fluoride (**6**) (2.69 g, 10.0 mmol) in CH_2Cl_2 (100 mL) and DMF (77 μL, 0.1 mmol) was added PBr_3 (1 M in CH_2Cl_2, 25.0 mL, 2.5 mmol) at room temperature. The reaction was stirred at room temperature overnight and then concentrated under reduced pressure. The residue was diluted with CH_2Cl_2 and quenched over ice. The organic phase was separated, washed with saturated aqueous sodium bicarbonate, brine, dried over magnesium sulfate, filtered and concentrated to afford the crude product as oil. The residue was purified by silica gel chromatography (0–50% EtOAc/heptane) to give compound **7** (1.85 g, 56%) as a white solid. ^{1}H NMR (400 MHz, $(CD_3)_2SO$) δ 8.24 (1H, d, $J = 8.20$ Hz), 8.20 (1H, s), 7.83 (1H, d, $J = 8.20$ Hz), 4.81 (2H, s) ppm. ^{19}F NMR (376 MHz, $(CD_3)_2SO$) δ 58.89 (s, 1F) ppm. ^{13}C NMR (126 MHz, $(CD_3)_2SO$) δ 148.8, 136.9, 133.3, 132.2 (d, 2 JCF = 30.24 Hz), 130.1, 120.6, 31.2 ppm. IR (neat): 3210, 1584, 1557, 1406, 1269, 1203, 1150, 1118, 1030, 302, 885, 841, 768, 713, 663, 637, 570, 535 cm^{-1}. GC–MS: m/z calcd for $C_7H_5Br_2FO_2S$ [M]: 329.8361; found: 329.8.

2.4. To a mixture of *tert*-butyl (2-amino-5-hydroxyquinazolin-4-yl) carbamate (**4**) (1.1 g, 4.0 mmol), and 2-bromo-4-(bromomethyl) benzenesulfonyl fluoride (**7**) (1.46 g, 4.4 mmol) in DMF (20 mL) was added Et_3N (1.62 g, 2.23 mL, 16.0 mmol) at room temperature. The reaction was heated at 60 °C for 16 h. After cooling to room temperature, the reaction was diluted with EtOAc. The organic layer was washed with water, saturated aqueous ammonium chloride, and brine, dried over magnesium sulfate, filtered and concentrated. The resulting residue was purified twice by silica gel (0–20% MeOH/EtOAc)

to give the title compound (**8**) (0.52 g, 25%) as a yellow solid. ^{1}H NMR (500 MHz, $(CD_3)_2SO$): δ 9.61 (1H, s), 8.38 (1H, d, $J = 1.47$ Hz), 8.35 (1H, d, $J = 8.07$ Hz), 8.00 (1H, d, $J = 8.07$ Hz), 7.55 (1H, t, $J = 8.31$ Hz), 7.01 (1H, dd, $J = 8.56$, 0.73 Hz), 6.83 (1H, d, $J = 7.58$ Hz), 6.58 (2H, s), 5.38 (2H, s), 1.27 (9H, s) ppm. ^{19}F NMR (470 MHz, $(CD_3)_2SO$): δ 58.54 (s, 1F) ppm. ^{13}C NMR (126 MHz, $(CD_3)_2SO$): δ 160.3, 156.9, 155.7, 155.3, 149.1, 146.2, 136.6, 133.8, 133.2, 132.7 (d, 2 JCF = 23.94 Hz), 129.5, 120.9, 119.1, 103.8, 102.5, 80.4, 69.9, 28.0 ppm. IR (neat): 3332, 1749, 1612, 1571, 1510, 1437, 1421, 1365, 1250, 1213, 1143, 1103, 1031, 994, 810, 778, 695, 665, 625, 592, 562, 544, 531 cm^{-1}. HRMS (ESI+) *m/z*: calcd for $C_{20}H_{20}BrFN_4O_5S$ $[M+H]^+$: 527.0395; found: 527.0387.

2.5. A microwave vial equipped with a stir bar was charged with *tert*-butyl (2-amino-5-((3-bromo-4-(fluorosulfonyl)benzyl)oxy)quinazolin-4-yl)carbamate (**8**) (0.24 g, 0.45 mmol), tributyl(ethnyl)stannate (0.43 g, 1.37 mmol), anhydrous toluene (4.0 mL) and anhydrous DMSO (4.55 mL). The reaction was degassed by sparging with argon gas for 10 min. [1,1′-bis(di-*tert*-butylphosphino)ferrocene]dichloropalladium(II) (0.059 g, 0.09 mmol) was added and reaction was heated in the microwave at 110 °C for 45 min. The reaction was diluted with EtOAc and filtered through celite twice. The solvent was concentrated under reduced pressure to give crude tert-butyl (2-amino-5-((2-ethynyl-4-(fluorosulfonyl)-benzyl)oxy)quinazolin-4-yl)carbamate which was used directly in the next step.

2.6. The residue was diluted with hydrochloric acid (4 M in dioxane, 1.5 mL, 6 mmol) and stirred at room temperature for 1 h. The residue was diluted in DMSO (1 mL) and purified by reverse-phase HPLC using a Kinetex pentafluorophenyl column 21.2 × 100 mm, 5 μm; Mobile phase A: 0.05% TFA in water (v/v); Mobile phase B: 0.05% TFA in acetonitrile (v/v); gradient (75:25 to 65:35), flow 25 mL/min to give title compound 4-(((2,4-Diaminoquinazolin-5-yl)oxy)methyl)-3-ethynylbenzenesulfonyl fluoride 2,2,2-trifluoroacetate (SF-p1-yne, Fig. 4) (12 mg, 5%) as white solid. ^{1}H NMR (500 MHz, $(CD_3)_2SO$): δ 12.48 (1H, s, br, TFA), 8.97 (1H, s), 8.63 (1H, s), 8.20 (1H, d, $J = 8.31$ Hz), 8.04 (1H, d, $J = 1.47$ Hz), 7.98–7.64 (2H, s, br), 7.83 (1H, d, $J = 8.31$ Hz), 7.63 (1H, t, $J = 8.31$ Hz), 6.98 (1H, d, $J = 8.07$ Hz), 6.91 (1H, d, $J = 8.31$ Hz), 6.54 (0.25H, s, TFA), 5.63 (2H, s), 5.01 (1H, s), 2.54 (s, DMSO) ppm. ^{19}F NMR (470 MHz, $(CD_3)_2SO$): δ 60.52 (s, 1F), −75.33 (s, 3.74F, 1.25 equivalent of TFA) ppm. ^{13}C NMR (126 MHz,

$(CD_3)_2SO$): δ 162.2, 155.9, 154.2, 145.1, 141.8, 136.0, 134.3, 132.7 (d, 2 JCF = 22.68 Hz), 130.7, 128.6, 121.2, 109.4, 107.11, 100.1, 90.6, 77.8, 68.3 ppm. ^{1}H NMR (500 MHz, CD_3OD) δ 8.18 (1H, d, J = 8.59 Hz), 7.99 (1H, s), 7.81 (1H, d, J = 8.20 Hz), 7.70 (1H, t, J = 8.39 Hz), 7.01 (2H, t, J = 8.20 Hz), 5.62 (2H, s), 4.29 (1H, s), 2.55 (s, DMSO) ppm. ^{19}F NMR (470 MHz, (CD_3OD): δ 58.20 (s, 1F), −76.95 (s, 3.74F, 1.25 equivalent of TFA) ppm. ^{13}C NMR (126 MHz, CD_3OD) δ 164.7, 158.1, 156.3, 145.6, 143.1, 137.7, 135.9 (d, 2 JCF = 23.94 Hz), 135.6, 132.0, 129.4, 124.0, 110.8, 108.9, 101.9, 89.6, 79.0, 70.7, 40.6 (trace DMSO) ppm. IR (neat): 3291, 3105, 2361, 1682, 1613, 1401, 1253, 1210, 835, 801, 722, 687, 579, 561, 542, 528 cm^{-1}. HRMS (ESI+) m/z: calcd for $C_{17}H_{13}FN_4O_3S$ $[M+H]^+$: 373.0765; found: 373.0767.

5. Protocols

5.1 Covalent labeling of recombinant DcpS

Now with the sulfonyl fluoride probe SF-p1 in-hand, we initially wanted to confirm covalent labeling of recombinant DcpS in vitro.

3.1. Incubate 0.5 μM recombinant DcpS with 1.5 μM SF-p1 in 50 mM Tris buffer with 1 mM TCEP at room temperature. Take samples at 15, 30, 45, and 75 min for intact mass measurement.

3.2. Determine protein masses by LC-MS using an Agilent 1100 HPLC system connected to a Waters LCT Premier XE mass spectrometer. Solvents for HPLC: A, 0.1% formic acid in water; B, 0.1% formic acid in acetonitrile. LC conditions: 0–1 min, isocratic at 2% solvent B; 1–22.5 min, 2–75%B running on a Higgins Analytical PROTO 300 C4 column (5 μM particle: 100 mm × 0.5 mm: p/n RS-10M5-W045) with a flow rate of 0.02 mL/min. The retention time of the DcpS protein is 17.5 min.

3.3. Rate of adduct formation between DcpS and SF-p1 is plotted using the MS intensity from the previous step using the following equation:

$$\%\text{DcpS} - \text{probe adduct} = \text{adduct intensity}/(\text{adduct intensity} + \text{apo DcpS intensity}) \times 100\%$$

As shown in Fig. 5A, SF-p1 achieves approximately 50% DcpS labeling after 20 min incubation.

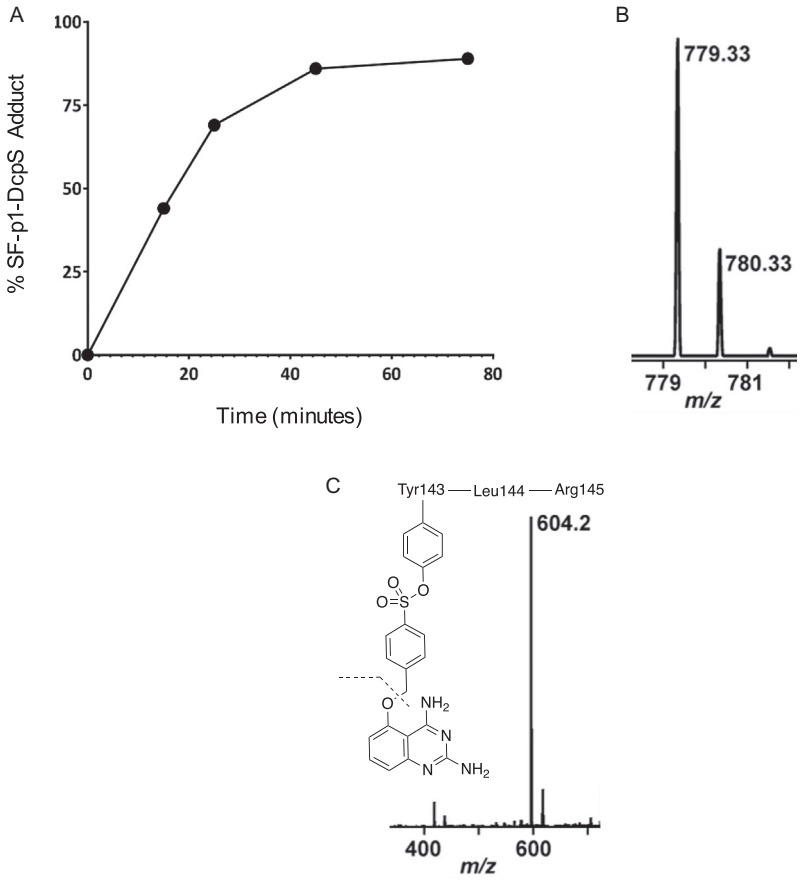

Fig. 5 (A) Rate of DcpS-probe adduct formation detected by LC-MS. (B) Tryptic peptide Tyr143-Leu144-Arg145 modified at Tyr143 (*m/z* 779.33). (C) MS/MS of the tryptic peptide, *m/z* 604.2 resulting from benzyl ether cleavage.

3.4. For peptide mapping experiments, incubate 0.15 mL of 0.5 μM DcpS, that was labeled by 1.5 μM SF-p1, with 0.60 mL ethanol at −80 °C for 48 h. Then centrifuge at 14,000 rpm for 10 min. Remove the supernatant, and dry the sample in a centrifugal concentrator. Resuspend the dried sample in 0.02 mL of 8 M urea and 10 mM iodoacetamide in phosphate-buffered saline solution (PBS) and incubate at room temperature for 30 min. Following a 5-h incubation with 0.5 μg trypsin, samples are then analyzed on an LTQ Orbitrap XL mass spectrometer. A unique tryptic peptide of DcpS Tyr143-Leu144-Arg145 modified at Tyr143 was identified (Fig. 5B, *m/z*

779.33). MS/MS of this species supported the structural assignment (Fig. 5C, neutral loss of the diaminoquinazoline fragment resulting from benzyl ether cleavage, m/z 604.2)

Tip: we skipped the standard DTT reduction step, since DcpS contains no disulfide bonds and milder sample processing conditions are required due to the chemical lability of the sulfonyl ester linkage.

These preliminary experiments confirmed that the location of the sulfonyl fluoride electrophile within the DAQ template is appropriate for protein labeling at the Tyr143 residue in the mRNA cap-binding site as predicted. Having established sulfonyl fluoride probe engagement of the functional site of the target enzyme, we next progressed the clickable, covalent DAQ (SF-p1-yne) to live cell experiments, where the terminal alkyne moiety enabled cycloaddition with biotin-azide and subsequent enrichment and analysis of the probe-DcpS adduct.

5.2 Labeling of DcpS in live cells

4.1. Thaw frozen human peripheral blood mononuclear cells (StemCell Technologies), transfer to 10 mL RPMI medium with 10% FBS, and centrifuge at 300 g for 5 min. Following aspiration of the medium, resuspend cells in 3 mL 100% FBS and incubate at 37 °C for 1 h. Wash cells with 30 mL PBS, and then centrifuge at $300 \times g$ for 5 min. Resuspend cells in 10 mL RPMI with 0.1% FBS.

Tip: 25 million cells are required for a sufficient signal after enrichment. In addition, cell clumps need to be removed by a BD Falcon Cell Strainer (40 μm Nylon) prior to the probe or inhibitor treatment (otherwise significant cell loss is observed).

4.2. Seed 1 mL cells per well in a 6-well plate with 25 million cells per sample. Add SF-p1-yne to the cells and incubate at room temperature for 20 min. Then spin the cells at $1000 \times g$ for 1 min, and wash twice with 1 mL PBS to remove excess probe.

4.3. Lyse cells with 50 μL lysis buffer (25 mM Tris-HCl pH 7.4, 150 mM NaCl, 1 mM EDTA, 1% NP-40 and 5% glycerol) with brief sonication to disrupt the nuclei. Remove cell debris by centrifugation for 1 min at $10{,}000 \times g$, and then transfer the supernatant to a 1.5 mL Eppendorf tube.

4.4. Perform click chemistry with cell lysate using the Click-iT® kit from Life Technologies. Specifically, add 100 μL of 80 μM biotin-azide in buffer A, briefly vortex, and then add 10 μL of 40 mM $CuSO_4$, and

vortex. Add 10 μL additive 1 solution and vortex. After 2–3 min, add 20 μL of additive 2, vortex, and then rotate end-over-end at room temperature for 1 h.

Tip: click reagents need to be stored at −20 °C after reconstitution in water.

4.5. Add 500 μL of 6 M urea made in the lysis buffer to the click reaction mixture and then add 150 μL high capacity streptavidin agarose beads (Thermo Fisher) and incubate at room temperature for 1 h. Centrifuge at 1000 × *g* for 1 min and wash three times with 1 mL 3 M urea in lysis buffer. Elute proteins off the beads by adding 100 μL of 2XLDS sample dye with reducing agent and heat to 95 °C for 5 min.

4.6. Separate proteins on 4–12% Bis-Tris protein gels, transfer to a PVDF membrane, and then detect DcpS by immunoblot (anti-DcpS antibody from Sigma HPA039632) using chemiluminescent SuperSignal West Femto substrate (Thermo Fisher).

Tip: Femto substrate needs to be used here due to the relatively weak DcpS signals following enrichment.

5.3 Competition labeling and quantification of target engagement

5.1. Incubate human PBMCs with varying concentrations of RG3039 (0.3 nM–1 μM) for 1.5 h, followed by a 20 min incubation with 1 μM SF-p1-yne. Then lyse the cells, perform click chemistry and streptavidin enrichment as described in steps 4.3–4.6.

5.2. Calculate DcpS occupancy signals by comparing DcpS signals from RG3039 treated samples to the signal from the "no inhibitor" sample. Fit the data to the following equation to obtain OC_{50}:

$$Y = \text{Bottom} + (\text{Top} - \text{Bottom})/(1 + 10\text{^}((\text{Log}OC_{50} - X)\text{*Hill Slope}))$$

Where Y is the percentage of DcpS signals after normalizing to the "no inhibitor" samples, X is the logarithm of the inhibitor concentration, the Hill Slope describes the "steepness" of the curve, "Top" and "Bottom" are plateaus in the units of the Y axis, and OC_{50} is the concentration at which the inhibitor achieves 50% occupancy of the protein target.

Western blot images and the occupancy curve for RG3039 are shown in Fig. 6. RG3039 displayed an OC_{50} of 11 nM for DcpS. This work validates RG3039 as a potent ligand of the mRNA cap-binding site of DcpS in living human primary cells.

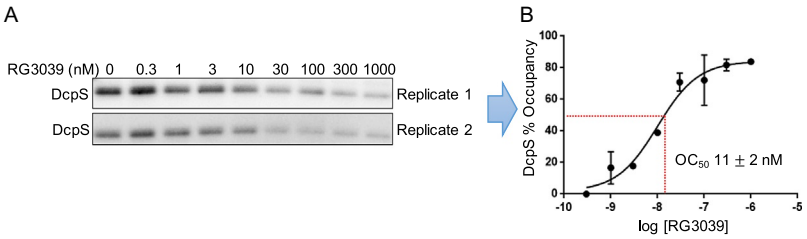

Fig. 6 (A) Western blot images of dose-dependent RG3039 inhibition of DcpS enrichment using SF-p1-yne in human PBMCs. (B) RG3039-DcpS occupancy curve in PBMCs.

6. Conclusions

Here, we have described a conceptual basis for target validation using reactive chemical probes and exemplified a broadly applicable strategy to assess drug-target engagement in living cells. We strongly urge the drug discovery community to adopt these techniques to build the necessary confidence in translational pharmacology required for successful target validation. Sulfur(VI) fluoride exchange chemistry is finding a renaissance in medicinal chemistry and chemical biology research that is underpinned by its magical reactivity (aqueous stability combined with specific and context-dependent amino acid engagement). The chemical probe-based technology detailed here leverages the emerging innovations in sulfonyl fluoride chemical biology and reports the first example of rationally targeting a specific tyrosine residue in a protein through the development of a covalent inhibitor.

The DAQ inhibitors of DcpS, such as the clinical candidate RG3039, were recently confirmed as lysosomotropic compounds, which complicates the assessment of their pharmacology (Gopalsamy et al., 2017). The results described here validate the annotated target as relevant to this chemotype in human primary cells. Potent DcpS inhibitors with improved physicochemical properties that lack lysosomal accumulation were shown to possess in vivo efficacy in a mouse model of SMA, thus providing further confidence in the proposed molecular mode of action (Cherry et al., 2017). However, more research is required to further elucidate the link between DcpS inhibition and amelioration of disease-relevant phenotypes in the model. Recently, DcpS was identified as a target of interest for the treatment of acute myeloid leukemia (using RG3039 as a pharmacological inhibitor) and the technology described here provides an opportunity to build PK-PD for this indication (Yamauchi et al., 2018).

We expect functional chemical probes will continue to be widely used to ensure that novel therapeutic targets are appropriately validated. However, the approach should be used in conjunction with orthogonal technologies such as the label-free cellular thermal shift assay (CETSA) to provide further confidence in the results (Savitski et al., 2014). Importantly for the research described here, CETSA was also used to measure DAQ-DcpS occupancy in live cells and the values obtained were almost identical to those using the sulfonyl fluoride-based method (Xu et al., 2016). Nevertheless, it should be noted that although CETSA continues to make considerable technical advances, a significant change in melting temperature upon ligand binding is not always observed (false negatives), and membrane proteins are particularly difficult proteins to assess. Chemical labeling methods directly measure drug-target engagement for practically any protein of interest that reacts with the probe. The functional chemical probe approach also enables binding site identification using MS peptide mapping experiments, as highlighted here.

A related use of sulfonyl fluoride covalent chemical probes includes the stabilization of difficult-to-crystallize proteins, resulting in useful structural information that informs rational drug design (Glukhova et al., 2017; Liu et al., 2016). A future application of the approach described may include target identification of small molecule hits in phenotypic screens when using quantitative MS analytical techniques. One can foresee even wider applications of this chemistry in biomedical research, including bioconjugation (such as the development of cleavable linkers to polyethylene glycol that improve the PK of protein therapeutics) and molecular biology (to enhance crosslinking-based sequencing technologies for instance). Sulfur(VI) fluoride chemical biology will continue to drive a deeper understanding of molecular pharmacology by augmenting the toolkit of protein labeling chemistry.

Acknowledgments

We thank Kieran Geoghegan, Lee Roberts, Erik Hett, Robert Kyne, Ariamala Gopalsamy, Arjun Narayanan, Mihir Parikh and Ralph Robinson for their essential contributions to this research and the development of sulfonyl fluoride chemical biology.

References

Ashoor, R., Yafawi, R., Jessen, B., & Lu, S. (2013). The contribution of lysosomotropism to autophagy perturbation. *PLoS One*, *8*(11), e82481. https://doi.org/10.1371/journal.pone.0082481.

Bunnage, M. E., Chekler, E. L., & Jones, L. H. (2013). Target validation using chemical probes. *Nature Chemical Biology*, *9*, 195–199.

Cherry, J. J., DiDonato, C. J., Androphy, E. J., Calo, A., Potter, K., Custer, S. K., et al. (2017). In vitro and in vivo effects of 2,4 diaminoquinazoline inhibitors of the decapping

scavenger enzyme DcpS: Context-specific modulation of SMN transcript levels. *PLoS One*, *12*(9), e0185079. https://doi.org/10.1371/journal.pone.0185079.

Cravatt, B. F., Wright, A. T., & Kozarich, J. W. (2008). Activity-based protein profiling: From enzyme chemistry to proteomic chemistry. *Annual Review of Biochemistry*, 77, 383–414. https://doi.org/10.1146/annurev.biochem.75.101304.124125.

Dong, J., Krasnova, L., Finn, M. G., & Sharpless, K. B. (2014). Sulfur(VI) fluoride exchange (SuFEx): Another good reaction for click chemistry. *Angewandte Chemie (International Edition in English)*, *53*(36), 9430–9448. https://doi.org/10.1002/anie.201309399.

Drewes, G., & Knapp, S. (2018). Chemoproteomics and chemical probes for target discovery. *Trends in Biotechnology*. https://doi.org/10.1016/j.tibtech.2018.06.008.

Garcera, A., Bahi, N., Periyakaruppiah, A., Arumugam, S., & Soler, R. M. (2013). Survival motor neuron protein reduction deregulates autophagy in spinal cord motoneurons in vitro. *Cell Death & Disease*, *4*, e686. https://doi.org/10.1038/cddis.2013.209.

Glukhova, A., Thal, D. M., Nguyen, A. T., Vecchio, E. A., Jörg, M., Scammells, P. J., et al. (2017). Structure of the adenosine A. *Cell*, *168*(5), 867–877.e813. https://doi.org/10.1016/j.cell.2017.01.042.

Gopalsamy, A., Narayanan, A., Liu, S., Parikh, M. D., Kyne, R. E., Fadeyi, O., et al. (2017). Design of potent mRNA decapping scavenger enzyme (DcpS) inhibitors with improved physicochemical properties to investigate the mechanism of therapeutic benefit in spinal muscular atrophy (SMA). *Journal of Medicinal Chemistry*, *60*(7), 3094–3108. https://doi.org/10.1021/acs.jmedchem.7b00124.

Hett, E. C., Xu, H., Geoghegan, K. F., Gopalsamy, A., Kyne, R. E., Menard, C. A., et al. (2015). Rational targeting of active-site tyrosine residues using sulfonyl fluoride probes. *ACS Chemical Biology*, *10*(4), 1094–1098. https://doi.org/10.1021/cb5009475.

Jarecki, J., Chen, X., Bernardino, A., Coovert, D. D., Whitney, M., Burghes, A., et al. (2005). Diverse small-molecule modulators of SMN expression found by high-throughput compound screening: Early leads towards a therapeutic for spinal muscular atrophy. *Human Molecular Genetics*, *14*(14), 2003–2018. https://doi.org/10.1093/hmg/ddi205.

Jones, L. H. (2015). Cell permeable affinity- and activity-based probes. *Future Medicinal Chemistry*, 7(16), 2131–2141. https://doi.org/10.4155/fmc.15.100.

Jones, L. H. (2016). An industry perspective on drug target validation. *Expert Opinion on Drug Discovery*, *11*(7), 623–625. https://doi.org/10.1080/17460441.2016.1182484.

Kolb, H. C., Finn, M. G., & Sharpless, K. B. (2001). Click chemistry: Diverse chemical function from a few good reactions. *Angewandte Chemie (International Edition in English)*, *40*(11), 2004–2021.

Liu, S., Dakin, L. A., Xing, L., Withka, J. M., Sahasrabudhe, P. V., Li, W., et al. (2016). Binding site elucidation and structure guided design of macrocyclic IL-17A antagonists. *Scientific Reports*, *6*, 30859. https://doi.org/10.1038/srep30859.

Liu, Q., Sabnis, Y., Zhao, Z., Zhang, T., Buhrlage, S. J., Jones, L. H., et al. (2013). Developing irreversible inhibitors of the protein kinase cysteinome. *Chemistry & Biology*, *20*(2), 146–159. https://doi.org/10.1016/j.chembiol.2012.12.006.

Morgan, P., Van Der Graaf, P. H., Arrowsmith, J., Feltner, D. E., Drummond, K. S., Wegner, C. D., et al. (2012). Can the flow of medicines be improved? Fundamental pharmacokinetic and pharmacological principles toward improving phase II survival. *Drug Discovery Today*, *17*(9–10), 419–424. https://doi.org/10.1016/j.drudis.2011.12.020.

Narayanan, A., & Jones, L. H. (2015). Sulfonyl fluorides as privileged warheads in chemical biology. *Chemical Science*, *6*, 2650–2659.

Rostovtsev, V. V., Green, L. G., Fokin, V. V., & Sharpless, K. B. (2002). A stepwise huisgen cycloaddition process: Copper(I)-catalyzed regioselective "ligation" of azides and terminal alkynes. *Angewandte Chemie (International Edition in English)*, *41*(14), 2596–2599. https://doi.org/10.1002/1521-3773(20020715)41:14<2596::AID-ANIE2596>3.0.CO;2-4.

Sanman, L. E., & Bogyo, M. (2014). Activity-based profiling of proteases. *Annual Review of Biochemistry*, *83*, 249–273. https://doi.org/10.1146/annurev-biochem-060713-035352.

Savitski, M. M., Reinhard, F. B., Franken, H., Werner, T., Savitski, M. F., Eberhard, D., et al. (2014). Tracking cancer drugs in living cells by thermal profiling of the proteome. *Science*, *346*, 1255784.

Singh, J., Salcius, M., Liu, S. W., Staker, B. L., Mishra, R., Thurmond, J., et al. (2008). DcpS as a therapeutic target for spinal muscular atrophy. *ACS Chemical Biology*, *3*(11), 711–722. https://doi.org/10.1021/cb800120t.

Thurmond, J., Butchbach, M. E., Palomo, M., Pease, B., Rao, M., Bedell, L., et al. (2008). Synthesis and biological evaluation of novel 2,4-diaminoquinazoline derivatives as SMN2 promoter activators for the potential treatment of spinal muscular atrophy. *Journal of Medicinal Chemistry*, *51*(3), 449–469. https://doi.org/10.1021/jm061475p.

Tornøe, C. W., Christensen, C., & Meldal, M. (2002). Peptidotriazoles on solid phase: [1,2,3]-triazoles by regiospecific copper(i)-catalyzed 1,3-dipolar cycloadditions of terminal alkynes to azides. *The Journal of Organic Chemistry*, *67*(9), 3057–3064.

Xu, H., Gopalsamy, A., Hett, E. C., Salter, S., Aulabaugh, A., Kyne, R. E., et al. (2016). Cellular thermal shift and clickable chemical probe assays for the determination of drug-target engagement in live cells. *Organic & Biomolecular Chemistry*, *14*(26), 6179–6183. https://doi.org/10.1039/c6ob01078d.

Yamauchi, T., Masuda, T., Canver, M. C., Seiler, M., Semba, Y., Shboul, M., et al. (2018). Genome-wide CRISPR-Cas9 screen identifies leukemia-specific dependence on a pre-mRNA metabolic pathway regulated by DCPS. *Cancer Cell*, *33*(3), 386–400.e385. https://doi.org/10.1016/j.ccell.2018.01.012.